J Mater Sci (2017) 52:2007–2020

Growth of zinc oxide nanorod structures: pressure controlled hydrothermal process and growth mechanism

R. Vasireddi[1], B. Javvaji[1], H. Vardhan[1], D. R. Mahapatra[1,*], and G. M. Hegde[2]

[1] Department of Aerospace Engineering, Indian Institute of Science, Bangalore 560012, India
[2] Centre for Nano Science and Engineering, Indian Institute of Science, Bangalore 560012, India

Received: 21 June 2016
Accepted: 6 October 2016
Published online: 13 October 2016

ABSTRACT

Zinc oxide (ZnO) nanorods of various morphologies are grown on zinc substrate by pressure-assisted hydrothermal process and the growth mechanism is investigated with the help of molecular dynamics (MD) simulation results. Hydrothermally reacted ZnO_2 nanostructure bottom-up formation from Zn substrate is a useful process employed here. A systematic study on the role of process control parameters such as pressure and temperature on nanorod growth has been carried out. Correlation among the process parameters to form ordered nanostructures is established. The effect of pressure on the diameter and length of the grown ZnO nanorod structures is studied, which is precisely tunable. With a decrease in pressure from 500 to 400 kPa, the nanorod diameter is reduced by 22.2 %, while its length is increased by 24.8 %. At lower vapor pressure, the nanorod tips are sharper, whereas at higher vapor pressure they are flat. These variations along with a detailed analysis of MD simulations helps us hypothesize that pressure plays an important role in governing the diffusion of oxygen atom onto zinc surface and generating wurtzite phase. Simulation results clearly show that ZnO nanorods lift off due to their interaction with the Zn atoms on the substrate and the resulting forces.

Introduction

Synthesis of precisely controlled nanostructures using a simple low-cost method is an important topic of interest due to wide range of applications [1–4]. In most of the chemical methods of nanofabrication, the growth of nanostructure starts with the deposition or precipitation of a seed nanoparticle by the agglomeration of atoms [5]. As a result, the size and shape of the nanostructure are primarily determined by such nucleation processes. Thermodynamically, the nanostructure grows in shape and size, which minimizes the free energy, and it grows in a direction by maximizing the energy release rate and thereby having a maximum non-equilibrium force component in that particular direction. One important

Address correspondence to E-mail: droymahapatra@aero.iisc.ernet.in

DOI 10.1007/s10853-016-0489-0

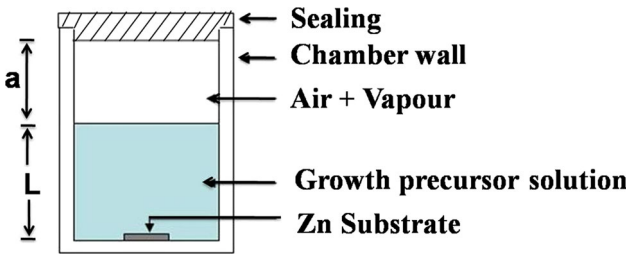

Figure 1 Schematic view of the hydrothermal chamber.

aspect that can affect the shape of the nanostructure is the reaction kinetics of the process. Nanostructures in the form of nanotubes, nanorods, nanowires, nanocubes, nanosprings, nanodisks, and dendrites have been grown by researchers in the recent years [6]. Spindle-shaped nanostructures grow in an environment of medium reactant concentration which promotes an isotropic growth in three dimensions [7]. Nanostructures in elongated shapes and rods are formed at higher reactant concentrations [8].

Zinc oxide is a direct wide-band gap (~3.37 eV) semiconductor having a large excitonic binding energy (~60 meV) at room temperature. It possesses useful thermal, chemical, structural, and optoelectronic properties. As a tetrahedrally bonded semiconductor, ZnO is a strong piezoelectric crystal. It has a significant electro-mechanical coupling property [9–12]. In the last few years, many new approaches have been developed to synthesize zinc oxide nanorods and other forms [13]. These developments are heavily promoted by the introduction of new technologies and emerging requirements of these nanostructures in various fascinating applications. A wide verity of methods such as pulsed laser deposition [14], atomic layer deposition [15], radio frequency sputter deposition [16], solution phase route [17], thermal decomposition [18], oxidation of zinc [19], reduction followed by the oxidation of zinc sulfide [20], electrodeposition [21], reactive evaporation method [22], and hydrothermal route reported in a recent study [23–25] have been employed to synthesize ZnO nanostructures.

Various ZnO nanostructures, including nanotowers, nanorods, nanovolcanoes, nanotubes, and nanoflowers, have been obtained by the hydrothermal technique [26]. The reported hydrothermally grown ZnO exhibits high optical quality, depending on growth conditions [27]. However, these methods of preparation of ZnO nanorods still carry some drawbacks, such as the requirement of sophisticated,

Figure 2 FESEM images of the grown ZnO nanostructures for various different growth conditions: **a** H_2O at 400 kPa, **b** H_2O at 430 kPa, **c** H_2O at 500 kPa, **d** 0.2 M of H_2O_2 at 400 kPa, **e** 0.2 M of H_2O_2 at 430 kPa, **f** 0.2 M of H_2O_2 at 500 kPa, **g** 0.4 M of H_2O_2 at 400 kPa, **h** 0.4 M of H_2O_2 at 430 kPa, **i** 0.4 M of H_2O_2 at 500 kPa, **j** 0.6 M of H_2O_2 at 400 kPa, **k** 0.6 M of H_2O_2 at 430 kPa, **l** 0.6 M of H_2O_2 at 500 kPa, **m** 0.8 M of H_2O_2 at 400 kPa, **n** 0.8 M of H_2O_2 at 430 kPa, and **o** 0.8 M of H_2O_2 at 500 kPa at constant temperature and time, respectively. ▶

expensive equipments and reactants. Other approaches demand rigorous experimental conditions and result in low yield. Also, there is no single route which can grow ZnO of different sizes and shapes. Therefore, there is a need to develop simple and scalable routes for the synthesis of ZnO nanostructures with effective control parameters.

We present here a simple and pressure-assisted hydrothermal catalytic approach to obtain scalable and tunable ZnO nanorod-based morphologies on zinc substrate, which one can further integrate or transfer on a device. A correlation is established involving the pressure in the hydrothermal chamber, reaction pressure for growth, structural dimension, temperature, and species concentration. The proposed method is of importance, since it enables the growth of nanorods directly on zinc thin-film substrate. Further, the proposed method can be scaled up if the process parameters such as pressure, temperature, chamber size, reaction duration, and concentration of the reactants can be controlled to fine-tune the geometrical attributes, area or volume densities, and morphologies of the grown structures. Moreover, the fundamental mechanism responsible for the supply of Zn from the bottom substrate, supply of reactive species from the solution interface, and ultimately the growth of long rod is poorly understood. Molecular dynamics (MD) simulations are performed considering these chemical and physical conditions to confirm our hypothesis regarding the growth mechanism and lift-off of nanorod from substrate.

Materials and methods

ZnO nanorod structures were grown on zinc substrates by the hydrothermal oxidation route. The schematic of the hydrothermal chamber is shown in

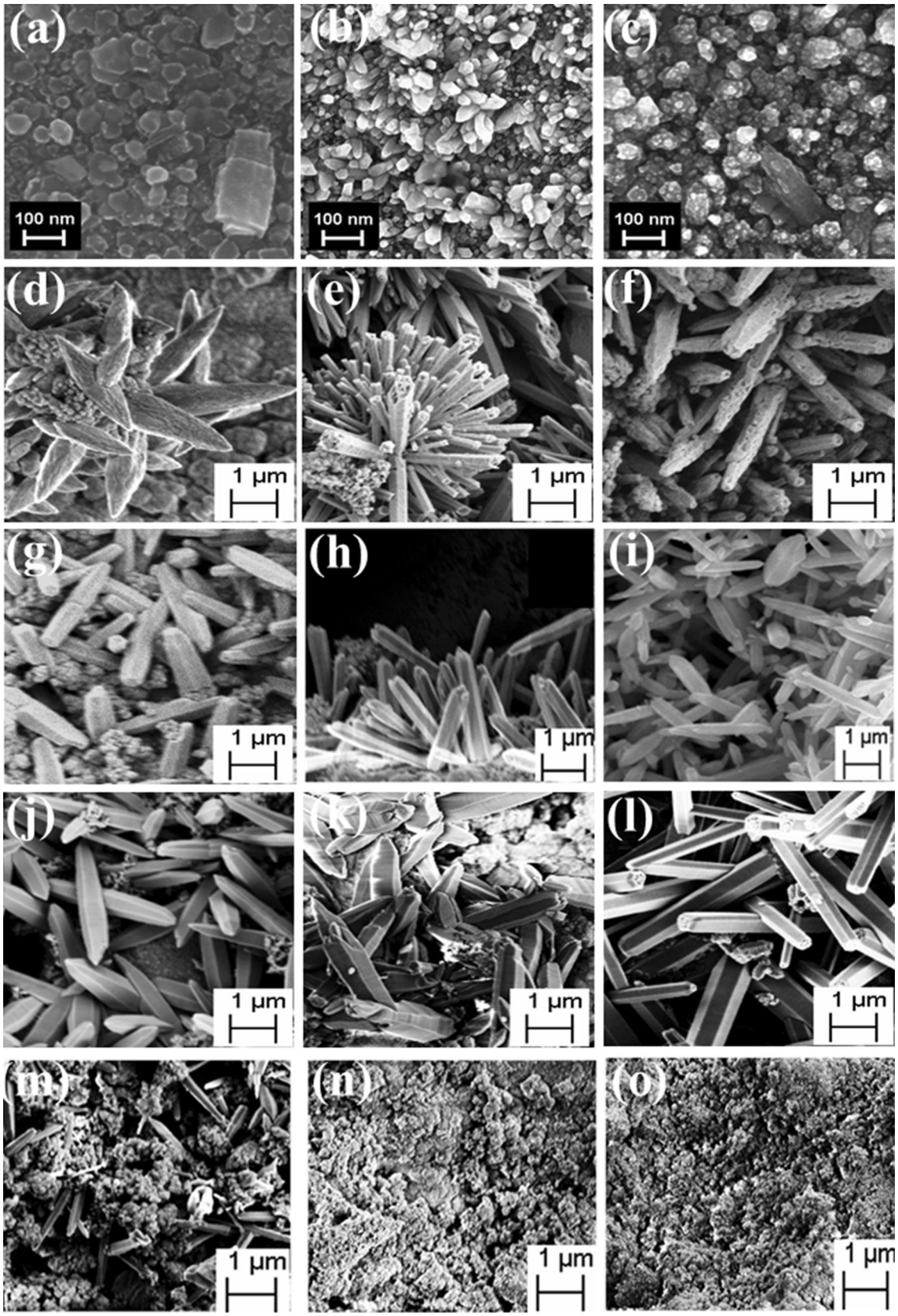
(a)
100 nm
(b)
100 nm
(c)
100 nm
(d)
1 μm
(e)
1 μm
(f)
1 μm
(g)
1 μm
(h)
1 μm
(i)
1 μm
(j)
1 μm
(k)
1 μm
(l)
1 μm
(m)
1 μm
(n)
1 μm
(o)
1 μm

Table 1 Reaction conditions for each sample of grown ZnO nanostructures

Solution used	Liquid volume			Temperature (°C)	Time (*h*)
	30 ml (400 kPa)	40 ml (430 kPa)	50 ml (500 kPa)		
Dist. H_2O	Fig. 2a	Fig. 2b	Fig. 2c	100	14
0.2 M H_2O_2	Fig. 2d	Fig. 2e	Fig. 2f	100	14
0.4 M H_2O_2	Fig. 2g	Fig. 2h	Fig. 2i	100	14
0.6 M H_2O_2	Fig. 2j	Fig. 2k	Fig. 2l	100	14
0.8 M H_2O_2	Fig. 2m	Fig. 2n	Fig. 2o	100	14

Fig. 1. It is made of sealed Teflon bottle which is subjected to external heating in a furnace.

Ultra-pure zinc substrate is first cleaned by ultrasonication in acetone for 5 min and then with distilled water to make the surface free from contaminants and any surface adsorbents before loading in the hydrothermal chamber. The thin-film substrate is placed centrally at the base of the hydrothermal chamber. The substrate is of size 10 mm × 10 mm × 0.25 mm. The chamber has the inner dimensions of 47 mm diameter and 81 mm depth. Distilled water is poured into the hydrothermal chamber up to a predefined volume in order to achieve the required vapor pressure and temperature. Before heating, the hydrothermal chamber is sealed completely by its Teflon screw cap. After sealing, the chamber is kept in a standard muffle furnace and heated at 100 °C for 14 h. The ZnO nanorods grow due to the oxygen atoms available in the chamber and the reaction-induced driving force overcoming the pressure. As mentioned above, this pressure is controlled by the liquid column height above the zinc substrate, which in turn defines the volume of the liquid, volume of air initially present in the chamber, and temperature. To optimize the growth of ZnO nanostructure, we perform the experiment with varying the ratio of liquid volume to air volume, temperature, and the duration of hydrothermal reaction. Hydrogen peroxide is used in different concentrations as a catalyst to understand its role on the growth of ZnO nanostructure. The morphologies of ZnO nanorods were characterized using field emission scanning electron microscopy (FESEM) (Zeiss Ultra55). Phase identification and quantitative phase analysis were done using X-ray diffraction (XRD) (PANalytical X'PERT PRO). X-rays were generated from a Cu target with a CuKα radiation wavelength of 1.54 Å.

We now explain the reaction mechanism. In the present experiment, pure water is found to oxidize zinc to form ZnO nanorods by the following reactions:

$$Zn + 2H_2O \rightarrow Zn(OH)_2 + H_2 \uparrow, \quad (1)$$

$$Zn(OH)_2 \rightarrow ZnO + H_2O. \quad (2)$$

The Zn atoms on the surface of Zn substrate form higher surface energy and therefore they act as active sites. They first react with water. Consequently, there is an increase in the concentration of zinc ions and hydroxide ions. These ions react to form $Zn(OH)_2$. Finally, ZnO is formed by the dehydration of $Zn(OH)_2$ which occurs under the hydrothermal conditions with a specific range of pressure and temperature [28]. The addition of H_2O_2 leads to a higher reaction rate where hydroxide ions are formed by redox reaction of hydrogen peroxide as follows:

$$H_2O_2 + 2e^- \rightarrow 2OH^-. \quad (3)$$

A hydrogen peroxide molecule is reduced by electrons provided by the zinc atom (Eq. 1). The zinc atom oxidized by water forms a zinc ion and further combines with hydroxyl ion [26, 29]:

$$Zn \rightarrow Zn^{2+} + 2e^-, \quad (4)$$

$$2H^+ + 2e^- \rightarrow H_2 \uparrow, \quad (5)$$

$$Zn^{2+} + 2OH^- \rightarrow ZnO + H_2O. \quad (6)$$

After applying heat for certain duration to maintain the liquid–vapor equilibrium state, the solution is cooled down to room temperature. We compare the characteristics of ZnO nanorod formation for varying H_2O_2 concentrations in the range of 0–0.6 M. We are able to tune various parameters of nanostructures with repeatable morphologies and establish correlations with growth parameters.

Results and discussion

Figure 2 shows the FESEM images of nanorods grown under various different conditions (see Table 1). Nanorods with needle-shaped tips form at low pressure, whereas the tips are flat when the

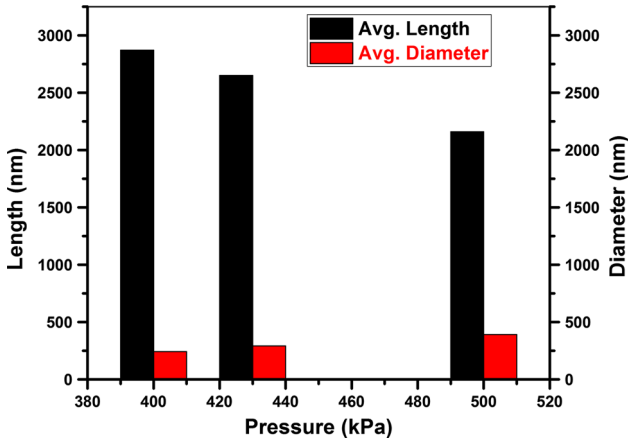

Figure 3 Nanorod length and diameter with varying pressures at the same H_2O_2 concentration of 0.6 M.

pressure is high. We hypothesize that according to the ZnO structure described above in "Materials and methods" Section, the flat tips indicate an incomplete growth of the nanostructures within the time available during heating and cooling ramps. This is due to the fact that more number of OH^- ions will be present on the flat tips of the ZnO nanostructure. These hydroxyl ions require more number of zinc ions which are needed to be supplied during the initial stages of growth from the bottom substrate. Growth duration of about 14 h under the above conditions is found optimal for the pointed tips. Various different morphologies are obtained by adding various different vapor-to-liquid volume ratios containing 0.2 M (Fig. 2d–f), 0.4 M (Fig. 2g–i), and 0.6 M (Fig. 2j–l) of H_2O_2. From the scanning electron microscope images shown in Fig. 2j–l for varying pressures (400–500 kPa), we have calculated the average length and average diameter using ImageJ software at a concentration of 0.6 M of H_2O_2. The calculated values of diameter and length are plotted in Fig. 3 for pressures in the range of 400–500 kPa. From Fig. 3, it is found that the nanorod diameter is reduced by 22.2 %, while its length is increased by 24.8 % with a decrease of pressure.

It can be seen that the morphologies of the ZnO nanostructures change from needle tip type to flat or blunt top hexagonal nanorods and the average rod length and diameter increase. This is because the rate of nucleation of ZnO changes with the increase of H_2O_2 concentration [30]. These results clearly indicate that the addition of H_2O_2 has a significant effect in controlling the shape of ZnO nanostructures.

Various distinct nanostructures (flower like, bridge with dendrite, hexagonal tip type, etc.) are obtained with specific control parameters as shown in Fig. 4. The structure shown in Fig. 4a resembles the morphology of a flower-like structure, in which the long

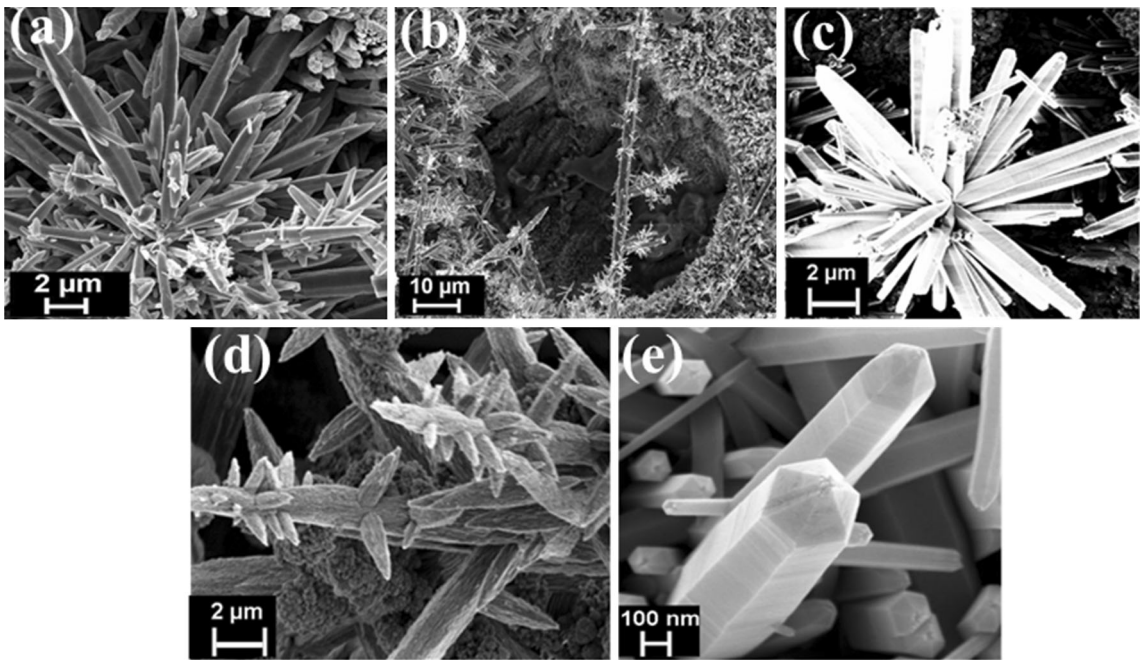

Figure 4 Special structural patterns of ZnO nanorods grown in a solution containing **a** 0.65 M H_2O_2 at 417 kPa, **b** 0.65 M H_2O_2 at 431 kPa, **c** 0.6 M H_2O_2 at 500 kPa, **d** 0.2 M H_2O_2 at 431 kPa, and **e** 0.6 M H_2O_2 at 431 kPa.

nanorods with sharp tips are pointing radially outward with small angular deviations; shorter nanorods in large quantity are self-assembled into flower-like structure. This nanorod structure has promising application in field emission and gas sensing devices where higher rod density or surface area is important. The structure shown in Fig. 4b resembles a bridge with dendrite substructures grown on its surface, which may be used as semiconductor interconnects. Figure 4c shows a flower-like structure, with nanorods diverging from one small site, but these nanorods are somewhat thicker with rounded tip.

Figure 4d shows solid wedge-type structures with sharp tips. Strong dendritic resemblance and secondary branching can be seen. Vertically oriented hexagonal nanorods with sharp hexagonal tips are shown in Fig. 4e. A general conclusion is that with a higher concentration of H_2O_2, nanorod branching is significant when the pressure is increased; at very high pressure, the tip tends to become flattened, whereas at a sufficiently high H_2O_2 concentration of 0.6 M and lesser pressure we obtain nanorods of very good quality nanorods.

These nanostructures have potential applications in photovoltaic devices, piezoelectric energy harvesting, sensors, and nanoelectronic semiconductor devices. The growth mechanisms of these structures can be understood by considering the fact that ZnO wurtzite crystals exhibit different growth rates for different planes. In stable wurtzite form, zinc oxide crystallizes with hexagonal shape correspond to the space group C6mc. In such configuration, the lattice parameters are as follows: $a = 0.325$ and $c = 0.521$ nm [31]. This structure consists of planes that are composed of tetrahedrally coordinated O^{2-} and Zn^{2+} ions. Eventually, there is a stacking of these planes in an alternating pattern along c-axis. A crystal of ZnO has three fast growth directions: $\langle 2\bar{1}\bar{1}0\rangle$, $\langle 01\bar{1}0\rangle$, and $\pm[0001]$. The basal plane is the most common polar plane. Planar defects and twins have been found to occur parallel to the (0001) plane. However, dislocations are rarely observed in this crystal. Reaction enthalpy on the Zn substrate surface is expected to increase growth in $\langle 01\bar{1}0\rangle$ direction due to the increment in pressure. Previously published studies [32] indicate that OH^- ions influence strongly and specifically the Zn^{2+} ions on the (0001) surface and thus inhibit the growth along [0001] and force the growth to take place along the $\langle 01\bar{1}0\rangle$ direction. Because of these different growth rates, which are also functions of the H_2O_2 concentration and pressure, the controlled synthesis of a specific nanostructure can be realized. Nanorod dimensions are measured for various nanostructures under various growth conditions and compared in Fig. 5. Note that the values shown in Fig. 5 are obtained from the averages of six samples. Error bars in Fig. 5 indicate the standard deviation of length and diameter for the samples considered. The distribution of the coefficient of variation, i.e., the ratio of standard deviation to mean (in the order of 0.2), is not significant. Hence, from Figs. 2 and 5, it is clear that the dimensions of the grown ZnO nanorods have good correlation with the solution concentration and pressure (vapor pressure) in the hydrothermal chamber.

Hydrothermally grown ZnO nanorods are further characterized using XRD to understand the structural compositions. The presence of crystalline phases was confirmed from XRD data (shown in Fig. 6) in the nanorod array grown on Zn film prepared with distilled H_2O and 0.6 M H_2O_2 solution with a vapor-to-liquid volume ratio of 40:70 in the chamber. The peaks were first determined for unreacted Zn substrate (Fig. 6a). With respect to these peaks, the substrate with ZnO nanorods grown on them was analyzed by XRD. After the pure zinc substrate was treated with distilled water in 40:70 vapor-to-liquid volume ratio, only a small part of the substrate was covered with oxide phase, with sites randomly distributed over the surface. The entire surface of the Zn substrate was exposed, and therefore some peaks appearing for Zn substrate are also observed in the XRD pattern of the reacted substrate. However, since the crystalline Zn phase amount reduced due to the hydrothermal growth of ZnO nanorods, the intensity dropped for the peaks corresponding to the crystalline Zn. The first strongest peaks in Fig. 6b for H_2O are located at $2\theta = 54.55°$ and 43.35° which belong to (102) and (101) planes. The residual peak for the sample shown in Fig. 6b appears at $2\theta = 34.57°$, which matches closely with the angle ($2\theta = 34.58°$) corresponding to the peak expected for the hexagonal phase of ZnO, but the most dominant peaks are observed for pure crystalline Zn. This is for growth in H_2O without catalyst and clearly the vertical growth is not prominent as shown in Fig. 2c. From Fig. 2a–c, Zn substrate is oxidized (form Zn–O seeds) with

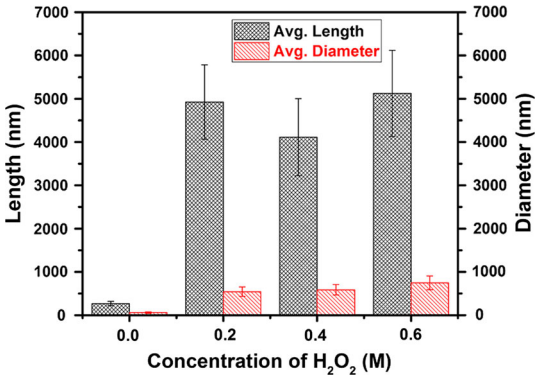

Figure 5 Comparison of nanorod dimensional features at various different concentrations of H_2O_2 and a pressure of 500 kPa.

respect to the liquid volume or pressure and it further develops the hexagonal rods. Better growth has taken place at higher concentrations of catalyst (Fig. 2l), which clearly shows growth along (002) direction as shown in Fig. 6c and further reconfirmed in Fig. 6d by extracting the grown nanorods in powder form.

The sharp diffraction peaks clearly show that the as-prepared ZnO nanorods have high crystallinity. However, the new peaks in XRD pattern that appeared for the sample grown with 0.6 M H_2O_2 have also shown some cubic phases of ZnO_2 as shown in Fig. 6c. Figure 6d illustrates the XRD pattern of the nanorod powder extracted from the grown nanostructure substrate. It can be observed clearly that the extracted nanorods consist of wurtzite crystal structure of ZnO. In Fig. 6d, the sharp peaks are at the 2θ values of 31.8°, 34.5°, 36.3°, 47.6°, 56.6°, 62.9°, 66.4°, 68.1°, 69.1°, 72.6°, and 77.1° corresponding to the lattice planes (100), (002), (101), (102), (110), (103), (200), (112), (201), (004), and (202), respectively. The sharp diffraction peaks clearly show that the as-prepared ZnO nanorods have high crystallinity. These ZnO nanorods have the lattice constants of $a = 0.32$ and $c = 0.52$ nm and exhibit hexagonal symmetry. All the XRD peaks (Fig. 6d) were indexed and matched well with the standard hexagonal structure of ZnO (JCPDS card no. 36-1451) [33].

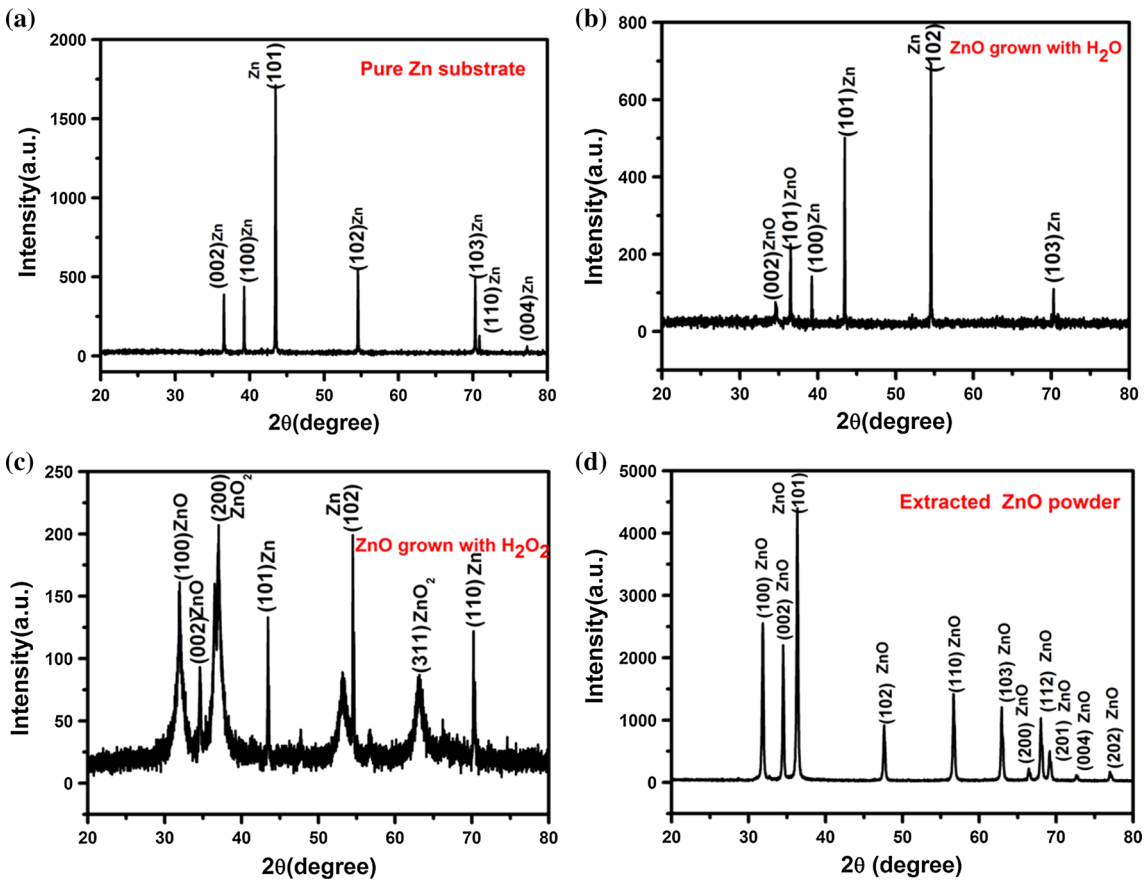

Figure 6 XRD peaks for **a** pure zinc substrate, **b** Zn substrate having nanorods grown with distilled water (Fig. 2c), **c** Zn substrate having nanorods grown at 0.6 M H_2O_2 at 500 kPa (Fig. 2l) and **d** extracted grown nanorods in powder form.

We analyzed the morphological changes of ZnO nanostructures due to the variation of H_2O_2 concentration and the role of process parameters such as pressure and temperature on nanorod growth. The fundamental mechanism responsible for the supply of Zn from the substrate at the bottom, the supply of reactive species from the solution interface, and ultimately the growth of very long rod is intriguing and poorly understood. A general hypothesis is that Zn atoms from the substrate chemically interact with the oxygen supplied from liquid solution, which leaves ZnO as a major product of the chemical reaction. These ZnO clusters are condensed under the given hydrothermal conditions of pressure and temperature, which results in a ZnO wurtzite structure. Our experimental results show that nanorod growth under certain specified conditions occurs along [0001] direction, indicating that there may be a pull-over force on Zn atoms on the substrate in this direction. Such a force pulls the Zn atoms which are reacting with oxygen, and it leads to an upward growth of ZnO nanorods. Further confirmation of ZnO growth mechanism is verified with our atomistic model which is discussed in detail at the end of the paper.

Nucleation is the first step toward oxide precipitation process in most of the metals. The initial surface oxidation of metals occurs through nucleation, growth [34], and merging of oxide islands. Oxidation on the metal surface involves a process of surface diffusion, due to which oriented nuclei are formed. Structure of the oxide can be governed by a control over the nucleation process. During oxidation of metal, oxide islands nucleate, which is initiated by the reaction of gaseous oxygen with the metal substrate. The morphology and nanostructure of the oxide film can be tuned by applying suitable controls over the nucleation process. Control parameters such as vapor pressure, temperature, and reaction time should be optimal to maintain good distribution of length-scale parameters. After having studied the effect of all the above parameters in ZnO nanorod formation and size distribution experimentally, we observed that the pressure plays an important role in controlling the reaction enthalpy, which in turn controls the dimensional features at nanoscale. In the proposed method, the pressure is controlled by the liquid–vapor equilibrium in terms of volume and temperature. Additional control in terms of H_2O_2 concentration leads to a positive outcome.

Pressure generated over the zinc substrate is calculated using the thermodynamic properties of closed system. Let T_1 be the room temperature (300.15 K), T_2 the elevated temperature during growth (373.15 K in the present study), P_a the partial pressure of air, P_v the partial pressure of water vapor, P the total pressure, ρ the density of liquid, and V the volume of liquid solution in the chamber. In the open chamber at room temperature, the pressure is equal to the atmospheric pressure and the total pressure $P = P_a + P_v$, so that $P(T_1)$ is 101.325 kPa. From the standard steam table data, $P_v(T_1)$ is 3.564 kPa and $P_a(T_1)$ is 97.765 kPa. After a stable growth condition is reached, assuming an isothermal system, $P_a(T_2) = [P_a(T_1)]\,(T_2/T_1) = 121.54$ kPa. We obtain the pressure above $P(T_2)$ as 222.87 kPa. The cumulative pressure over the Zn substrate at growth temperature T_2 can be expressed as $P = P(T_2) + \rho g h$, where h is the liquid height in the chamber. Considering our system geometry, we correlate the total pressure to the length and diameter of the ZnO nanostructure as shown in Fig. 7. From Fig. 7a–b, the nanostructure lengths are in several microns, whereas the diameters are in several hundreds of nanometers with a maximum aspect ratio (length-to-diameter) of 7. Although the pressure dependence of ZnO nanorod dimensions and shape is very clearly based on the above analysis, however, a quantitative correlation among these parameters needs to be established. This is currently under-investigated and will be reported in the future.

The atomistic model we use to establish our hypothesis consists of a Zn substrate and a ZnO nanorod in a simulation box of length l_x (15 nm), width l_y (15 nm), and height l_z (25 nm). The details are shown in Fig. 8. One-fifth of the simulation box height is filled with hexagonal Zn substrate atoms from its bottom. We introduce a nucleated ZnO nanorod with wurtzite structure in [1000] orientation on the Zn substrate surface. The diameter D and length L of ZnO nanorod are taken as 5 and 10 nm, respectively. The nucleated nanorod and the substrate are separated by height h, which is to allow migration of reactive species. This simulation setting is used to understand the dynamics near the bottom of the ZnO nanorod and Zn substrate as a source of Zn into the growth reaction. The initial atomic configuration is created using the hexagonal close-packed crystal structure for Zn and wurtzite crystal lattice for ZnO. Initially, a small gap (h) called

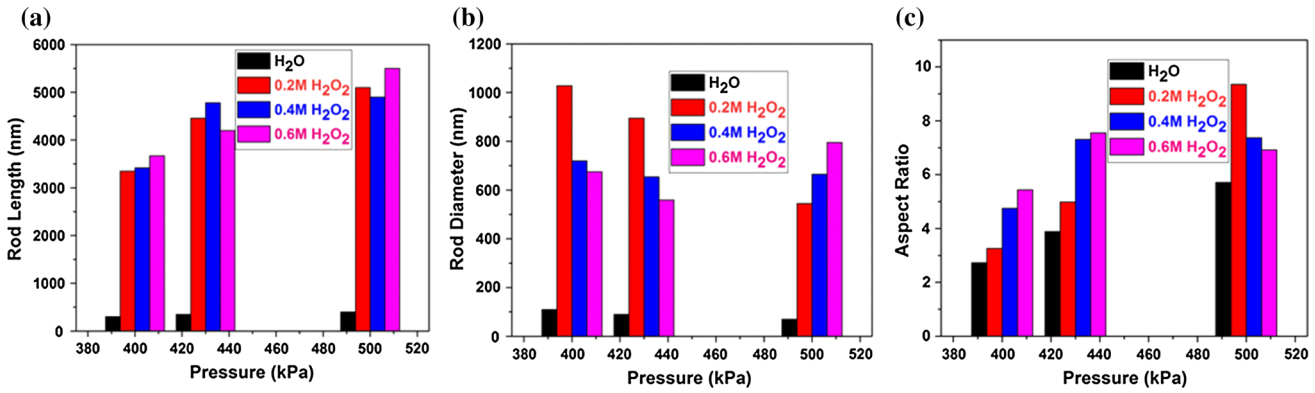

Figure 7 Quantitative characteristics of nanorod versus total pressure and variation in terms of **a** average length, **b** average diameter, and **c** average aspect ratio.

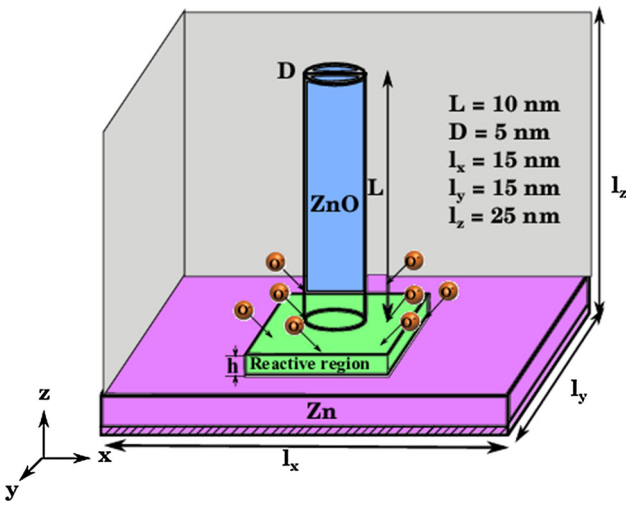

Figure 8 Schematic diagram showing the simulation box consisting of ZnO nanorod on Zn substrate and scheme for studying the dynamics of reactive species.

reactive region is kept for oxygen atom supply with a density at its room temperature. It is understood that the major reactive products from Eqs. (1)–(6) are hydroxyl (OH^-) ion and hydrogen (H_2) gas. The hydroxyl ion chemically interacts with the substrate Zn atom and produces ZnO seed. From Eq. (6), any two hydroxyl ions interact with each other and release water and oxygen ion in the presence of Zn. The remaining oxygen ions will interact with Zn and produce ZnO. In the simulations, we consider the supply of ionized oxygen molecules into the reactive region between Zn substrate and ZnO nanorod. Such a consideration allows the chemical reaction between substrate Zn and the ionized oxygen molecules. The simulation box consists of 63068 Zn atoms and 5156 O atoms. The interatomic interactions are modeled using charge-optimized many-body (COMB) potential with charge as a variable [35]. A recent study on the tensile properties of ZnO nanowire used an interatomic potential which involves the short-range atomic interactions along with fixed charge-based Columbic repulsions [36]. Such a fixed charge approximation is not sufficient to capture the variation of charge with respect to bond stretching between Zn and O, whereas COMB potential uses the variable charge approximation which explains the chemical reaction. According to COMB potential, the total potential energy E^{T} for the system of atoms is expressed as

$$E^{\mathrm{T}} = \sum_i E_{\mathrm{i}}^{\mathrm{self}}(q_i) + \sum_i \sum_{j \neq i} \left(E_{ij}^{\mathrm{short}}(r_{ij}, q_i, q_j) + E_{ij}^{\mathrm{Coul}}(r_{ij}, q_i, q_j) + E^{\mathrm{polar}}(r_{ij}, q_i) \right) + \sum_i \sum_{j \neq i} \left(E^{\mathrm{vdW}}(r_{ij}) + E^{\mathrm{barr}}(q_i) + \sum_{k(\neq i,j)} E^{\mathrm{corr}}(r_{ij}, \theta_{jik}) \right), \quad (7)$$

where i, j, and k are the atomic indices, q_i is the charge on atom i, r_{ij} is the distance between the atoms i and j, and θ_{ijk} is the angle subtending between atoms i, j, and k. E^{self} is the atomic ionization potential energy, E^{short} is the bond-order potential energy with a dependency over charge q, E^{Coul} is the Columbic interaction energy due to charged atoms, E^{polar} is the polarization energy, E^{vdW} is the non-bonding atomic interaction energy, E^{barr} is the charge exchange/transport barrier potential, and E^{corr} is the correction term in the potential due to angular orientation of the bonds. Detailed mathematical expressions can be found in Ref. [35].

The initial coordinates of the atomic system are supplied to an energy minimization algorithm along with a charge optimization scheme [37], which keeps the atoms in their minimum energetic positions in the sense of ensemble average over time. Initially, we assumed that the charge of Zn atoms in the substrate is zero and O atoms with a charge of $-0.28e$, and after simultaneous charge and energy minimization, charges on Zn and O atoms are $0.7e$ and $-0.7e$ (e is the electronic charge), respectively.

Total energy minimization leads to certain arrangement of O atoms close to the separation layer between the nucleated rod and the substrate. The Zn atoms on the surface of crystalline substrate have a lesser coordination number compared to the bulk Zn crystal, which leads to an ionization state of Zn atoms. O atoms near the Zn substrate are negatively ionized to maintain charge neutrality. After energy minimization, the system of atoms in the box along with the associated charges is subjected to a pressure of 500 kPa and a temperature of 373 K to simulate the hydrothermal condition of reaction. Temperature and pressure are maintained using the Nosé–Hoover thermostat and barostat, respectively. The equations of motion are integrated with a time step of 0.5 fs using velocity Verlet algorithm [38] along with Nosé–Hoover [39, 40] chain conditions for a period of 40 ps. All the simulations are carried out using the software code called LAMMPS [41]. Time-averaged quantities (atomic coordinates, charge, and forces on each atom) were calculated at the intervals of 10 ps. From this, we measured the bond length, bond angle, and charge variations, which confirmed ZnO wurtzite structure. Atomic-level force data are analyzed further to understand atomic diffusion and growth mechanism.

Before analyzing the growth process, first we need to understand the equilibrium characteristics of atomistic model. The atomistic model was equilibrated at a constant temperature of 373 K and the pressure of 500 kPa. In the equilibration process, the ensemble average values of pressure and temperature are noted at every 1 ps time interval. For the initial elapsed time less than 14 ps, rapid variations are observed in pressure and temperature. Due to the application of external conditions, a sudden change like this in the kinetic energy as well as the potential energy of the atomic system may be the reason for the transients. Redistribution of energy over atoms via atomic relaxation brings the system to a stable state. It is observed that the time taken for relaxation is about 14 ps. Thereafter, the simulation model is in a stable equilibrium state. With equilibrated atomic system as the initial configuration, we study the ZnO growth which will be discussed later.

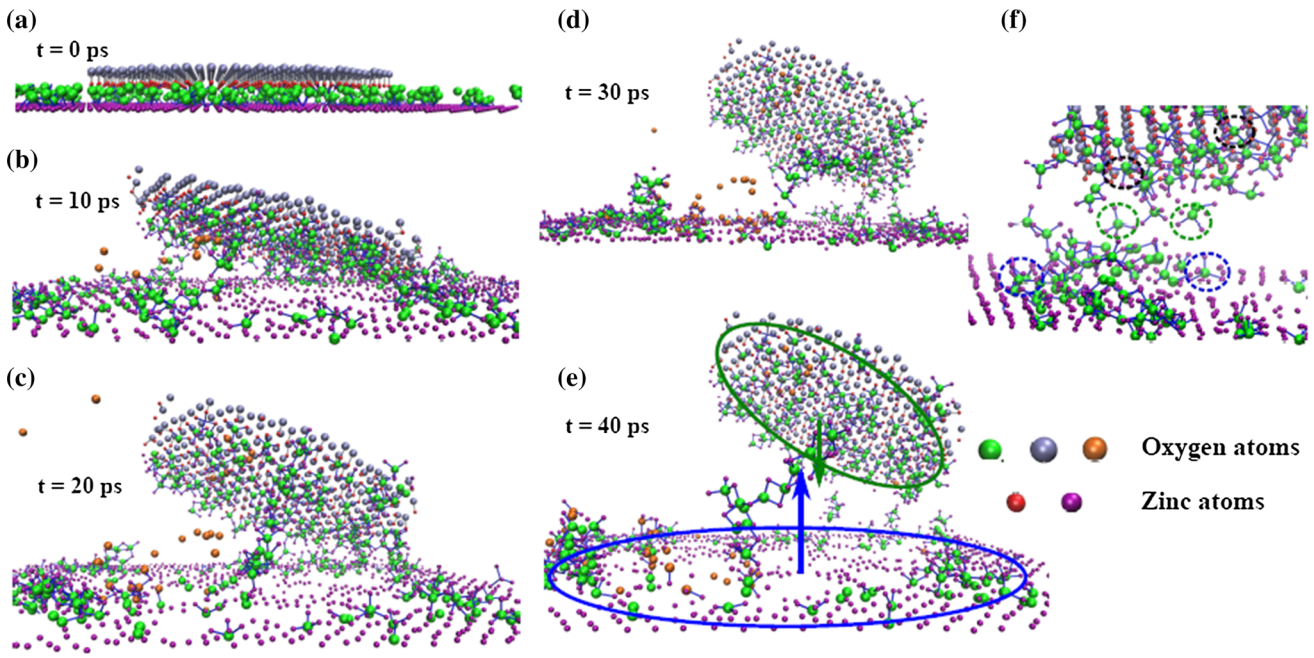

Figure 9 **a**–**e** Atomic configurations of ZnO nanorods on Zn substrate at different time instances. **f** Zoomed portion of the reactive area (**c**) between the nanorod and the substrate. Regions used for force calculations and the direction of force components are highlighted in (**e**).

Figure 9a–e presents the atomic snapshots in the simulation process. The analysis of atomic coordinates and charges reveals Zn atom bonding with two O atoms (Zn–O seed). Formation of Zn–O seed is confirmed by the numerical values of bond length, bond angle, and charges on the atoms. A group of atoms in the simulation model are selected and shown in the inset of Fig. 10a. The selected atoms are labeled as A, B, C, E, F, G, and H. Figure 10a shows the bond distance between successive atoms in this group. The Zn–O bond length is found to be 2.1 Å and it is nearly constant after 15 ps of elapsed time. Bond angle oscillates at 110° after attaining equilibrium (see Fig. 10b). Oxidation reaction involving atomic charge variation over time is confirmed from Fig. 10c. Initially, the charges for atoms A and B are 0.7 and −0.7, respectively, and for atoms C to G the values are zero. Note that atoms A and B are selected from the bottom of the ZnO nanorod. The interatomic potential considered here is a function of the charge variable. At each simulation step, charges on the atoms are calculated according to the current atomic configuration. As the atoms start displacing, charge equilibration algorithm optimizes the charge distribution. While relaxing the atomic system, the Zn substrate surface is charged (charges on atoms E and G are non-zero as shown in Fig. 10c at 2 ps). This is because the surface Zn atoms are having a smaller coordination number compared to bulk, which makes surface atoms to displace. Such a displacement causes an initial positive charge on Zn atoms. Similarly, O atoms are displaced by the thermal vibrational forces, which create initial negative charge on O atoms. Further, the oppositely charged atoms develop Coulomb attraction and Zn–O seeds are formed. However, these forces get equilibrated in the

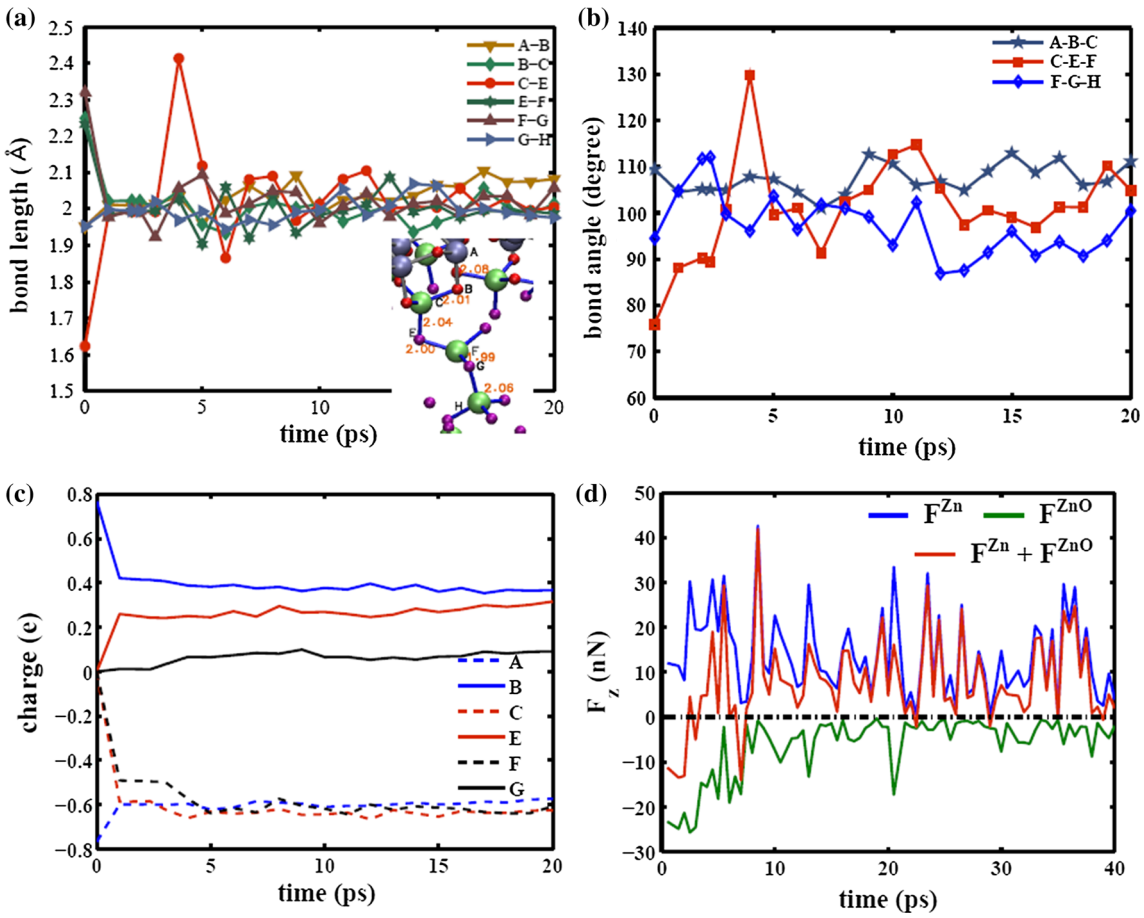

Fig. 10 **a** Variations of bond lengths with respect to time for the selected atomic configuration. *Inset* presents the assembly of selected atoms labeled as *A*, *B*, *C*, *E*, *F*, *G*, and *H*. **b** Variations of bond angles and **c** atomic charges with time. **d** Time variation of averaged force components from the cluster of atoms in Zn substrate and ZnO nanorod, which are participating in the chemical reaction. The sum of both the force components is also shown.

simulation process, which is reflected in the nearly constant nature of variation of charge and the vibration stability of Zn–O seeds.

Several Zn–O seeds are found in the atomic snapshot taken at 20 ps of elapsed time (Fig. 9c). We found that there are three types of seeds (highlighted in Fig. 9f): (1) free seeds, (2) substrate seeds, and (3) nanorod seeds. Free seeds are marked as green circles in Fig. 9f; which are free to bond with nanorod or substrate. Substrate seeds are marked as blue circles in Fig. 9f; where Zn–O seed is bonded with the top surface of the Zn substrate. The nanorod seeds are marked as black circles in Fig. 9f, where Zn–O seed is attached to the bottom surface of the nanorod. Note that Zn atoms in type 1 and type 2 seeds are from the Zn substrate. There is an important confirmatory result that the chemical reaction in our experiments creates a Zn–O seed, the condensation of which is guided by pressure and temperature.

From Fig. 9c, it is observed that there is an atomic bridge between the Zn substrate and the ZnO nanorods. The atomic configuration in this bridge confirms that the atoms are ordered according to ZnO wurtzite structure. Several small bridges are also found. Zn atoms in these bridges are drawn from the Zn substrate. This confirms that Zn substrate atoms create Zn–O seeds and these seeds condense at the bottom part of the nanostructure, which result in the growth of ZnO nanorods. We also found that there is tilting in the nanorods at ~20 ps (see Fig. 9c). As the atomic bridge grows, nanorod moves away from the Zn substrate and tilts. The tilt is due to the non-uniform growth of atomic bridges on the substrate. The non-uniform growth results from the disturbance due to the mismatch between the direction of convective heat transfer and the direction of O supply.

It is found that Zn atoms are lifting off from the substrate and this is the primary reason for the upward growth of the nanostructure. Consider a set of substrate atoms within the reactive region and their averaged z component of force (F^{Zn}) are calculated at periodic intervals of time. Atomic forces on ZnO nanorods along z direction (F^{ZnO}) are calculated and averaged near the bottom of the nanorod portion in the reactive region. It is observed that the time variation of F^{Zn} and F^{ZnO} is opposite to each other as shown in Fig. 10d. In Fig. 9e, the direction of forces and the regions used for force calculation are highlighted. The positive nature of F^{Zn} confirms that the Zn substrate atoms are lifting off from the surface. The lifted Zn atoms are in ionized state and interact with the O atoms; Zn–O seeds are formed followed by the condensation into ZnO nanorods in upward direction from the bottom. Condensation is understood from the bridge-like growth. As the time passes from 10 ps to 12 ps, the lift-off force decays, which is due to the reactive energy minimization. We further supplied oxygen atoms (orange color in Fig. 9c) at a time interval of 2 ps, which disturbs the energy minima. As a result, a rise in F^{Zn} is observed and ZnO nanorod is further separated upward from the Zn substrate. Zn and O ions form Zn–O seeds and are getting attached to the ZnO nanorod. The rise in F^{Zn} is sharp and started decaying between 12 to 14 ps. A fall in F^{Zn} represents the Zn–O seed attached to the recently grown part, which helps in bulging the same. The next rise in F^{Zn} is located at 14 ps, which corresponds to the increased growth. A continuous supply of oxygen atoms will lead to the rise and fall patterns of F^{Zn}. The positive sign of resultant force $F^{Zn} + F^{ZnO}$ ensures that the lift-off force is upward and Zn–O seed attachment will continue. Velocity (temperature) of the O atoms side way can also disturb the upward growth and can cause random structures or flower-like structure emerging from a single seed, which have been experimentally observed as discussed earlier.

Conclusions

We have presented a simple one-step, cost-effective, and environment-friendly hydrothermal scheme for the controlled growth of high-aspect ratio zinc oxide nanorods directly on zinc substrate. FESEM images have shown that the nanorods' dimensions and shapes vary with pressure and H_2O_2 concentration. Also, the materials grow into ZnO nanorods and acquire a high aspect ratio for higher hydrostatic pressure. Special cases where other complex morphologies can be formed are also shown and a mechanistic scheme behind this is analyzed. An empirical relation is formulated to estimate the pressure inside the hydrothermal chamber. Correlating with the classical mechanism of nucleation, we have predicted that at high pressure the oxygen atoms impact smaller surface area and diffuse widespread onto the zinc substrate as compared to that under low pressure. This governs the kinetics of wurtzite phase formation and evolution of shape and dimensional features of the nanorods. The molecular

structures of the solution composition are different at low and high temperatures, thus with a low-density structure at elevated temperatures. At high temperature, it also has high vapor pressure. Therefore, pressure plays a critical role in phase transformations at high temperature. In this context, we have demonstrated a simple methodology for controlled and tunable growth of ZnO nanorod structures on zinc substrate by controlling the pressure. The MD simulations performed in this work provide quantitative information toward the understanding of the role of pressure and temperature in the growth process, which is relevant for the fundamental understanding of the growth mechanism. The proposed method where lift-off of nanorod can be controlled precisely by various thermo-mechanical and reactive schemes is scalable to large-area ZnO nanorod growth and patterning.

Acknowledgements

The authors acknowledge the financial support of Aeronautics R&D Board, Government of India, under the ACECOST phase-III program to carry out this research.

References

[1] Huang MH, Mao S, Feick H, Yan H, Wu Y, Kind H, Weber E, Russo R, Yang P (2001) Room-temperature ultraviolet nanowire nanolasers. Science 292:1897–1899

[2] Keis K, Vayssieres L, Lindquist SE, Hagfeldt A (1999) Nanostructured ZnO electrodes for photovoltaic applications. Nanostruct Mater 12:487–490

[3] Minne SC, Manalis SR, Quate CF (1995) Parallel atomic force microscopy using cantilevers with integrated piezoresistive sensors and integrated piezoelectric actuators. Appl Phys Lett 67:3918–3920

[4] Shibata T, Unno K, Makino E, Ito Y, Shimada S (2002) Characterization of sputtered ZnO thin film as sensor and actuator for diamond AFM probe. Sens Actuators A 102:106–113

[5] Burda C, Chen X, Narayanan R, El-Sayed MA (2005) Chemistry and properties of nanocrystals of different shapes. Chem Rev 105:1025–1102

[6] Yan Y, Zhang Y, Meng G, Zhang L (2006) Synthesis of ZnO nanocrystals with novel hierarchical structures via atmosphere pressure physical vapor deposition method. J Cryst Growth 294:184–190

[7] Peng X, Wickham J, Alivisatos AP (1998) Kinetics of II–VI and III–V colloidal semiconductor nanocrystal growth: focusing of size distributions. Am Chem Soc 120: 5343–5344

[8] Peng X (2003) Mechanisms for the shape-control and shape-evolution of colloidal semiconductor nanocrystals. Adv Mater 15:459–463

[9] Zhao XQ, Kim CR, Lee JY, Heo JH, Shin CM, Ryu H, Chang JH, Lee HC, Son CS, Lee WJ, Jung WG, Tan ST, Zhao JL, Sun XW (2009) Effects of buffer layer annealing temperature on the structural and optical properties of hydrothermal growth ZnO. Appl Surf Sci 255:4461–4465

[10] Pal E, Hornok V, Oszko A, Dekany I (2009) Hydrothermal synthesis of prism-like and flower-like ZnO and indium-doped ZnO structures. Colloid Surf A 340:1–9

[11] Tong Y, Dong L, Liu Y, Zhao D, Zhang J, Lu Y, Shen D, Fan X (2007) Growth and optical properties of ZnO nanorods by introducing ZnO sols prior to hydrothermal process. Mater Lett 61:3578–3581

[12] Corso AD, Posternak M, Resta R, Baldereschi A (1994) Ab initio study of piezoelectricity and spontaneous polarization in ZnO. Phys Rev B 50:10715–10721

[13] Tiwary CS, Vishnu D, Kole AK, Brahmanandam J, Mahapatra DR, Kumbhakar P, Chattopadhyay K (2016) Stabilization of the high-temperature and high-pressure cubic phase of ZnO by temperature-controlled milling. J Mater Sci 51:126–137. doi:10.1007/s10853-015-9394-1

[14] Zhao Y, Jiang YJ, Fang Y (2007) The influence of substrate temperature on ZnO thin films prepared by PLD technique. J Cryst Growth 307:278–282

[15] Lim JM, Lee CM (2007) Effects of substrate temperature on the microstructure and photoluminescence properties of ZnO thin films prepared by atomic layer deposition. Thin Solid Films 515:3335–3338

[16] Akshaya KB, Pritam D, Indrani T, Sriparna C, Shyamal C (2015) Temporal wetting property of "micro" versus "nano" rods of ZnO grown using the pressure dependent aqueous solution method. New J Chem 39:8993–8998

[17] Yang J, Lang J, Yang L, Zhang Y, Wang D, Fan H, Liu H, Wang Y, Gao M (2008) Low-temperature growth and optical properties of ZnO nanorods. J Alloys Compd 450:521–524

[18] Zhang J, Sun L, Liao C, Yan C (2002) A simple route towards tubular ZnO. Chem Commun 262(2002):262–263

[19] Wang YW, Zhang LD, Wang GZ, Peng XS, Chu ZQ, Liang CH (2002) Catalytic growth of semiconducting zinc oxide nanowires and their photoluminescence properties. J Cryst Growth 234:171–175

[20] Hu JQ, Li Q, Wong NB, Lee CS, Lee ST (2002) Synthesis of uniform hexagonal prismatic ZnO whiskers. Chem Mater 14:1216–1219

[21] Badre C, Pauporte V, Turmine M, Dubot P, Lincot D (2008) Water-repellent ZnO nanowires films obtained by octadecylsilane self-assembled monolayers. Physica E 40: 2454–2456

[22] Yamamoto K, Nagasawa K, Ohmori T (2004) Preparation and characterization of ZnO nanowires. Physica E 24:129–132

[23] Zafar HI, Kimleang K, Martin E, Mohammad A, Muhammad A, Anees A, Magnus W (2013) Hydrothermal growth of vertically aligned ZnO nanorods using a biocomposite seed layer of ZnO nanoparticles. Materials 6:3584–3597

[24] Haili L, Shujie J, Shanshan B, Hongtao L, Shiyong G, Jinzhong W, Qingjiang Y, Fengyun G, Liancheng Z (2014) Precursor-controlled synthesis of different ZnO nanostructures by the hydrothermal method. Phys Status Solidi A 211:595–600

[25] Liu W, Huang Q, Huang T, Cao P, Han S, Jia F, Zhu D, Ma X, Lul Y (2016) Secondary growth" in hydrothermal synthesis of aligned ZnO nanostructures and its application in dye-sensitized solar cells. J Nanosci Nanotechnol 16(4): 4016–4022

[26] Tong Y, Liu Y, Dong L, Zhao D, Zhang J, Lu Y, Shen D, Fan X (2006) Growth of ZnO nanostructures with different morphologies by using hydrothermal technique. J Phys Chem 110:20263–20267

[27] Demyanets LN, Lyutin VI (2008) Status of hydrothermal growth of bulk ZnO: latest issues and advantages. J Cryst Growth 310:993–999

[28] Dalal SH, Baptista DL, Teo KBK, Lacerda RG, Jefferson DA, Milne WI (2006) Controllable growth of vertically aligned zinc oxide nanowires using vapour deposition. Nanotechnology 17:4811–4818

[29] Xu S, Wang ZL (2011) One-dimensional ZnO nanostructures: solution growth and functional properties. Nano Res 4:1013–1098

[30] Henni A, Merrouche A, Telli L, Walter S, Azizi A, Fenineche N (2015) Effect of H_2O_2 concentration on electrochemical growth and properties of vertically oriented ZnO nanorods electrodeposited from chloride solutions. Mater Sci Semicond Process 40:585–590

[31] Meyer B, Marx D (2003) Density-functional study of the structure and stability of ZnO surfaces. Phys Rev B 67:035403–035414

[32] Wang ZL (2004) Zinc oxide nanostructures: growth, properties, and applications. J Phys 16:R829–R858

[33] Shi L, Bao K, Cao J, Qian Y (2009) Growth and characterization of ZnS porous nanoribbon array constructed by connected nanocrystallites. Cryst Eng Comm 11:2308–2312

[34] Saunders RB, McGlynn E, Henry MO (2011) Theoretical analysis of nucleation and growth of ZnO nanostructures in vapor phase transport growth. Cryst Growth Des 11:4581–4587

[35] Liang T, Shan TR, Cheng YT, Devine BD, Noordhoek M, Li Y, Lu Z, Phillpot SR, Sinnott SB (2013) Classical atomistic simulations of surfaces and heterogeneous interfaces with the charge-optimized many body (COMB) potentials. Mater Sci Eng 74:255–279

[36] Wang W, Pi Z, Lei F, Lu Y (2016) Understanding the tensile behaviors of ultra-thin ZnO nanowires via molecular dynamics simulations. AIP Adv 6:035111

[37] Rappe AK, Goddard WA (1991) Charge equilibration for molecular dynamics simulations. J Phys Chem 95: 3358–3363

[38] Swope WC, Andersen HC, Berens PH, Wilson KR (1982) A computer simulation method for the calculation of equilibrium constants for the formation of physical clusters of molecules: application to small water clusters. J Chem Phys 76:637–649

[39] Nosé S (1984) A unified formulation of the constant temperature molecular dynamics methods. J Chem Phys 81:511–519

[40] Hoover WG (1985) Canonical dynamics: equilibrium phase-space distributions. Phys Rev A 31:1695–1697

[41] Plimpton S (1995) Fast parallel algorithms for short-range molecular dynamics. J Comp Phys 117:1–19